The Middle to Upper Palaeolithic transition in Hohlenstein-Stadel cave (Swabian Jura, Germany): A comparison between ESR, U-series and radiocarbon dating

M Richard, C Falguères, E Pons-Branchu, D Richter, T Beutelspacher, N J Conard, C-J Kind

The Middle to Upper Palaeolithic transition in Hohlenstein Stadel cave (Swabian Jura, Germany): a comparison between ESR, U-series and radiocarbon dating

Richard M.[1, 2], Falguères C.[2], Pons-Branchu E.[3], Richter D.[4], Beutelspacher, T.[5], Conard, N.J.[6,7], Kind C.-J.[8]

[1]Institut de Recherche sur les ArchéoMATériaux-Centre de Recherche en Physique Appliquée à l'Archéologie, UMR 5060, CNRS, Université Bordeaux-Montaigne, Maison de l'Archéologie, F-33607 Pessac, France.

[2]Département « Homme et Environnement », UMR 7194, CNRS, Muséum national d'Histoire naturelle, 1 rue René Panhard, F-75013 Paris, France.

[3]Laboratoire des Sciences du Climat et de l'Environnement, UMR 8212, CNRS, CEA, USVQ, Avenue de la Terrasse, F-91190 Gif-sur-Yvette, France.

[4]Department of Human Evolution, Max Planck Institute for Evolutionary Anthropology, D-04103 Leipzig, Germany.

[5]State Office for Cultural Heritage Baden-Württemberg, Alexanderstraße 48, D-72072 Tübingen, Germany.

[6]Tübingen/Senckenberg Center for Human Evolution and Palaeoecology, University of Tübingen, Sigwartstraβe 10, D-72074 Tübingen, Germany.

[7]Abteilung Ältere Urgeschichte und Quartärökologie, Institut für Ur- und Frühgeschichte und Archäologie des Mittelalters, University of Tübingen, Schloss Hohentübingen, D-72070 Tübingen, Germany.

[8]State Office for Cultural Heritage Baden-Württemberg, Berliner Straße 12, D-73728 Esslingen, Germany.

Abstract

The Swabian Jura is a key region for the Early Aurignacian. Sites such as Geißenklösterle, Hohle Fels and Hohlenstein-Stadel have produced the earliest evidence of figurative and musical art, such as ivory figurines and flutes made of bone and ivory. To date, ^{14}C and TL dating have been applied in the region, providing a precise chronology for the Upper Palaeolithic levels, especially the Aurignacian. At Hohlenstein-Stadel, Upper and late Middle Palaeolithic levels were dated using ^{14}C. This study focuses on the chronology of the

Middle Palaeolithic levels using ESR on herbivorous tooth enamel, in order to constrain the timing of the earliest human occupation at the cave, attributed to Neanderthals. An age was also obtained for the Early Aurignacian level, allowing a comparison with available ^{14}C ages. Furthermore, U-series dating was applied to three samples from a flowstone located at the base of the sequence, in order to provide a maximum age (*terminus post quem*) for the beginning of human occupation at the cave.

ESR results obtained on Middle Palaeolithic samples ranged from 40 ± 5 ka to 35 ± 3 ka (weighted mean ages), suggesting that these levels were deposited during a short period of time. The Early Aurignacian level (Geological Horizon, GH, Au) was dated to 34 ± 11 ka, in agreement with ^{14}C dates, despite a large error range due to the heterogeneity of the sedimentological environment. The flowstone overlying the oldest deposit at the base of the stratigraphy was dated to between 351 ± 10 ka (MIS 10-9) and 229 ± 10 ka (MIS 7), providing an age for the start of the karstic activity and a maximum age for the deposits, respectively.

These new chronological data confirm that Neanderthals occupied Hohlenstein-Stadel during MIS 3. Radiocarbon ages suggest that the replacement of Neanderthals by *Homo sapiens* occurred during a brief period of time, probably before or during Heinrich Stadial 4 (around 40-38 ka).

1. Introduction

Radiocarbon dating has been widely applied to date late Middle and Upper Palaeolithic sites, especially in Europe where the attribution of the transitional industries to Neanderthal and/or *Homo sapiens*, as well as the origin of Aurignacian, are still debated (e.g., d'Errico, 2003; Mellars, 2005; Conard and Bolus, 2006; Floss, 2017). For sites older than 45-50 ka, trapped-charge dating can be applied to date sediment (optically stimulated luminescence, OSL and electron spin resonance, ESR), heated flint (thermoluminescence, TL) and tooth enamel (ESR). Age determinations obtained from younger deposits (i.e., < 45 ka) using these methods can be compared with radiocarbon (^{14}C) ages, which is preferentially applied to such contexts, due to its precision and the abundance of organic material at archaeological sites. However, to date, only a few comparisons between ESR and ^{14}C dating have been published (e.g., Peresani et al., 2008).

The Swabian Jura is a region of low mountains located in southwestern Germany. The Lone and Ach valley cave complex (**Fig. 1**) ranks among the earliest Aurignacian occupations, attributed to *Homo sapiens*. Hohlenstein-Stadel (Swabian Jura, Germany) is a cave site known for producing early Aurignacian levels, dated to around 40-36 ka cal BP (Kind et al., 2014), in which an ivory-carved figurine, the *Löwenmensch* ("Lion-man"), was uncovered. Among the earliest examples of European figurative art attributed to *Homo sapiens*, its chronology, together with ivory carved figurines from other sites in the Swabian Jura (e.g., Hohle Fels, Vogelherd, Conard, 2003, 2009) has played a key role in the understanding of modern human dispersal and the origin of the Aurignacian (Conard and Bolus, 2003; Higham et al., 2012).

Prior to modern human occupation, Neanderthals were present in the cave, as suggested by the levels yielding Middle Palaeolithic artefacts associated with faunal remains with cut marks. Radiocarbon dating was applied to the late Middle and Upper Palaeolithic levels (Conard and Bolus, 2003; Hahn, 1977; Kind et al., 2014; Schmid, 1989). Here, ESR and U-series dating are applied to tooth enamel and a flowstone overlying the lowest level respectively, in order to complete the chronostratigraphic framework for the base of the archaeological sequence and to compare the results with ^{14}C ages obtained from the late Middle Palaeolithic and Early Aurignacian levels of Hohlenstein-Stadel.

2. Archaeological, chronostratigraphical and palaeoenvironmental contexts

Hohlenstein-Stadel is located near Asselfingen, 25 km from Ulm, in the Lone Valley (**Fig. 1**) in Baden-Württemberg (Southwest Germany). Excavations started under the direction of O. Fraas in 1861-62, and continued with R. Wetzel in 1937-39 and 1956-61 (see references in Kind et al., 2014). Archaeological material can be attributed to several cultural periods, ranging from the Middle Palaeolithic to the Mesolithic. In August 1939, fragments from the Lion-man were discovered, and reassembled by J. Hahn in 1969 (Hahn, 1971) and E. Schmid in 1987-88 (Schmid, 1989) (**Fig. 2**). Recent excavations were directed by C.-J. Kind between 2008 and 2013 in order to collect stratigraphic and archaeological data regarding the context of human occupation in the cave during the Late Pleistocene (Beutelspacher et al., 2010; Beutelspacher and Kind, 2011; Kind et al., 2014). During these investigations, further ivory fragments of the Lion-man figurine were discovered. Also, a test pit was dug in order to document the stratigraphy and correlate it with data from old excavations. The sequence features 15 geological horizons (GH), including 12 Middle Palaeolithic levels (from C to

K/M), and three Aurignacian levels (Ao, Am et Au) (**Fig. 3 and Tab. 1**), where the ivory pieces belonging to the lion-man were recently discovered (Kind et al., 2014). During the last excavations campaigns, about 600 artefacts were uncovered in the Middle Palaeolithic levels, which were dated to more than 40 ka BP by ^{14}C (Kind et al., 2014).

Radiocarbon dating was first applied to the Aurignacian levels, on material from the old excavations. Ages range from 37 to 35 ka cal BP (Conard and Bolus, 2003; Conard and Bolus, 2008; Hahn, 1977; Schmid, 1989) (see details in **Tab. SI1**). Recently, ^{14}C analyses using the ultrafiltration procedure were carried out on both Aurignacian and Middle Palaeolithic bones (Kind et al., 2014). The results indicate that the Aurignacian levels date to 40-36 ka cal BP (**Tab. 1**). For the late Middle Palaeolithic levels, ages range from ca 45 (GH D) to 43 ka cal BP (GH C), whereas the age obtained for GH E falls out of the calibration range (ca 46 ka BP) (**Tab. 1**).

With regard to the palaeoecological data, cave bear (*Ursus spelaeus*) is the dominant taxon in Hohlenstein-Stadel. The remains correspond to individuals that died during hibernation, and thus are not related to the human occupation of the cave (Krönneck et al., 2004). Hyena (*Crocuta spelaea*) is well represented, particularly in Middle Palaeolithic levels, thus indicating that humans and carnivores occupied the cave alternatively (Krönneck et al., 2004). Cave lion (*Panthera leo spelaea*), wolf (*Canis lupus*) and fox (*Vulpes/Alopex*) are also present (Kitagawa et al., 2012). Concerning herbivores, horse (*Equus ferus*) is the most represented species for both Middle and Aurignacian levels. Woolly rhinoceros (*Coelodonta antiquitatis*), reindeer (*Rangifer tarandus*), red deer (*Cervus elaphus*) and bison (*Bos/Bison*) remains also occur in Middle Paleolithic levels (Kitagawa et al., 2012). The presence of cold biotopes species confirms that humans were present in the cave during harsh climatic phases. Both chronological (^{14}C ages) and paleoenvironmental data seem to indicate that human occupation of the cave could be traced back to MIS 3.

3. Material and Methods

3.1. Sampling and preparation

Nine teeth were sampled from the sequence (**Fig. SI1**), starting from the base (GH K) up to the Aurignacian level (GH Au), allowing a comparison with ^{14}C ages for the upper part of the stratigraphy (**Tab. 2 and Fig. 3**). Apart from the rhinoceros tooth (HS09), all other

dated samples were attributed to equids. A flowstone overlying the sterile GH M, at the base of the sequence, was sampled and three phases were dated (**Fig. SI2**). Sediment from each dated geological horizon was collected for beta dose rate determination (**Tab. 2 and Fig. 4**). The beta dose rate received from the external part of the enamel was calculated from the U-content in the cement covering the equid teeth, and from the sediment for the rhinoceros sample (no cement).

The enamel, dentine and cement (in the case of the equid teeth) were separated mechanically and cleaned with an electric drill. A minimum thickness of 30 to 40 µm was removed from each side of the enamel to eliminate the contribution of alpha particles. The enamel was grounded and sieved to obtain a 100-200 µm granulometric fraction used for ESR measurements. However, due to the state of preservation of the enamel, which was more fragile for some of the teeth, the ESR analyses were conducted on the < 200 µm fraction (see **Tab.2** caption).

The flowstone underlying GH K-M was sampled using a circular saw. Three samples (S1, S3 and S4) were extracted in the laboratory using an electric drill for U-series ($^{230}Th/^{234}U$) analyses (**Fig. SI2**).

3.2. Irradiation and ESR analyses

Each enamel sample was split into 10 aliquots. Nine of them were irradiated at increasing doses (40, 60, 100, 160, 250, 400, 630, 1000, 1600 Gy) using a ^{60}Co gamma source allowing a panoramic irradiation (LABRA, CEA, Saclay, France), and one was kept intact to measure the natural ESR signal.

ESR analyses were conducted in the Muséum national d'Histoire naturelle (MNHN, Paris, France) using an EMX Bruker ESR spectrometer working at room temperature (19 °C). The measurements were repeated four times for each aliquot using the following parameters: 5 mW microwave power, 0.1 mT modulation amplitude, 12 mT scan range, 2 min scan time and 100 kHz modulation frequency. The equivalent doses were calculated from the enamel T1-B2 signal at g = 2.0018 (Grün et al., 2008) using a single saturation exponential (SSE) function (Yokoyama et al., 1985).

3.3. U-series analyses

Each dental tissue forming the teeth samples was analysed at the Laboratoire des Sciences du Climat et de l'Environnement (LSCE, Gif-sur-Yvette, France) using the chemical procedure for the separation and purification of uranium and thorium isotopes described in Richard et al. (2015). For the flowstone, the samples were prepared according to the chemical procedure published in Pons-Branchu et al. (2014). Measurements on dental tissues and calcite samples were performed using a Quadrupole ICP-QMS following Douville et al. (2010).

3.4. Beta dose rate determination

The sediments sampled from the section were weighed before and after drying in an oven for one week to estimate their water content (%weight). ^{238}U, ^{232}Th and ^{40}K contents were measured using a high-resolution, low-background Ge detector at the MNHN. Beta dose rate for HS 09 was derived from these values according to the conversion factors published by Adamiec and Aitken (1998) using the DATA program (Grün, 2009).

3.5. *In situ* gamma dosimetry

Most of the teeth analysed in this study were found during excavations, before the site was accessible for dosimetry. Since the original sedimentary matrix of the samples has been completely excavated, the gamma dose rate has to be reconstructed from measurements in the section.

The gamma and cosmic dose rates were recorded in each dated geological horizon using 25 single crystal α-Al_2O_3:C dosimeters (TLD-500K, manufactured at the Ural State Technical University of Ekaterinburg, Russia) (**Fig. 4**). A travel dosimeter was bleached when removing the dosimeters from the section, in order to subtract the dose recorded between the time of removal and measurement. Dosimeters were analysed according to the procedure described in Richter et al. (2010). Since teeth were located far from the section (Figs. SI3 et 7), a mean value was calculated per layer and use for the age calculation.

The cosmic dose rate is attenuated by the cave vault (around 14 m) and the sediment (0.8-2 m) thickness. It can be estimated to 40 ± 4 $\mu Gy.a^{-1}$ (Prescott and Hutton, 1994). However, it was not subtracted from the values recorded by the dosimeters because: i) the topography of the cave is thought to be largely unchanged since Late Pleistocene; ii) samples were collected in the deepest part of the cave, at tens of meters from the entrance; iii) the

difference to past cosmic dose rates is thus only the sediment which has been removed. Given the thickness of the cave roof, the difference of maximum 150 cm is negligible for the cosmic dose rate.

4. Results and discussion

ESR ages are presented in **Table 3** and **Fig. 5** with the 1 σ error range and were calculated using the DATA program (Grün, 2009). The following parameters were taken into account for computation: an alpha efficiency of 0.13 ± 0.02 (Grün and Katzenberger-Apel, 1994); Monte-Carlo beta attenuation factors (Brennan et al., 1997); a water content (weight %) of 0% for the enamel and of 7 ± 5% for the dentine and cement; a water content in the sediment assumed to 20 ± 5%. Measured water content ranged from 10% (GH M) to 30% (GH D2), with values close to 20% for GHs AU, D and E. Taking into account that water content is variable over time, we consider a value of 20 ± 5% as representative for the cave. However, as dosimeters were placed in the section, they recorded the gamma dose rate as a function of the water content for the time of measurement. Ages range from 46 ± 9 ka (GH K) to 34 ± 11 ka (GH Au).

U-series data (^{238}U content and $^{230}Th/^{234}U$, $^{234}U/^{238}U$ and $^{230}Th/^{232}Th$) are presented in **Tab. 4**. They are used to derive the dose rate related to the presence of uranium in the dental tissues incorporated during burial through the reconstruction of an U-uptake parameter, the "p-value" (Grün et al., 1988). The latter can range from -1, corresponding to an Early Uptake (EU), to a positive value, corresponding to a Recent Uptake (RU). The measured ^{238}U content in all the dental tissues is low, ranging from 0.003 ppm and 0.540 ppm. Consequently, it was not always possible to determine isotopic ratios, the ^{230}Th signal being too weak for ICP-QMS. When detectable, $^{234}U/^{238}U$ ratios are higher than 1, and $^{230}Th/^{234}U$ are lower than 1. Nonetheless, considering the small amount of U in the dental tissues, the associated dose rate is negligible (representing less than 2% of the annual dose) and thus the U-uptake mode does not affect the calculated ages. ESR ages were thus calculated by using the EU model (Bischoff and Rosenbauer, 1981). In this case, U is assumed to be incorporated soon after burial; the model derives the alpha and beta dose rates only from the ^{238}U measured.

^{238}U, ^{232}Th and ^{40}K content measured in the sediment samples are presented in **Tab. 5**. The radioelement content is lower in the upper GHs (Au, D and D2) than in the lower ones (GHs E and K) (**Tab. 6**). There is a positive correlation between the environmental dose recorded by the dosimeters and the U, Th and K contents measured in the sediment samples.

In-situ gamma dosimetry values are scattered, and unexpectedly high for a karstic environment, noticeably for the lowest levels (**Tab. 6 and Fig. SI3-7**). A mean value and associated standard deviation was calculated for each GH; extreme values that do not fall within the range of the standard deviation were excluded. The mean value and associated standard deviation excluding the extreme values were used to calculate the ages for GHs AU, D, D2 and E. For GH K, two out of four dosimeters recorded a higher dose, superior to 1300 µGy. Dosimeter N°55 (774 µGy) recorded a similar dose to the one measured in the sediment sample using laboratory gamma-ray spectrometry (739 µGy). This value was thus considered to be more representative than the mean value for this GH (1179 µGy), higher by a factor 3 than the mean dose rate recorded in GHs Au and D.

Tab. 3 presents the equivalent doses (D_e), annual doses and EU-ESR ages obtained for the teeth samples. Dose response curves are available in **Fig. SI8-SI16**. Due to the low U-content in all dental tissues, EU or RU ages cannot be distinguished. Equivalent doses are low, ranging from 10 to 37 Gy. The dose rate from the sediment ($\beta + \gamma$) and the cosmic contribution (40 $\mu Gy.a^{-1}$) range from 410 ± 134 (GH Au) to 1035 ± 98 $\mu Gy.a^{-1}$ (GH D2). The sum of the dental tissue contribution does not exceed 8 $\mu Gy.a^{-1}$, representing maximum 6% of the annual dose. Consequently, the dose rate depends mainly on the environmental dose. The precision of the ages is thus highly impacted by the large error range of the gamma dose. They range from 46 ± 9 ka (GH K) to 12 ± 1 ka (GH D2). The ages obtained for GHs D2 (HS 09, 12 ± 1 ka) and E (HS 05, 15 ± 3 ka) are inconsistent with the stratigraphic order and the cultural context of the deposits. Considering that the D_e are slightly higher than the ones obtained for the samples from the upper levels, this stratigraphic inversion might be related to the environmental gamma dose, i.e., the dosimeters could have been included in clay pockets. If we take into account the gamma dose derived from radioisotopes contents measured by laboratory gamma-ray spectrometry for the age calculation, ages are 26 ka (GH D2) and 23 ka (GH E). The difficulties in reconstructing the environmental dose rate, added to the fact that only one sample could be dated for each of these two levels, do not allow a reliable chronology for these two levels.

Table 7 presents the U-content, activity ratios, uncorrected and corrected U-series ages (2 σ) obtained from the flowstone samples located at the base of the sequence, overlying the sterile GH M. ^{238}U content is low, ranging from 58 to 160 ppb. $^{234}U/^{238}U$ ratios range from 1.088 ± 0.001 to 1.152 ± 0.005 and $^{230}Th/^{234}U$ ratios are close to 1. Corrected ages (using initial $^{230}Th/^{232}Th$ of the detrital fraction = 1.5 ± 50 %) range between 351 ± 10 ka (for the lower part, S4) and 229 ± 10 ka (for the upper part, S1). They indicate that the precipitation of

the flowstone took place likely during MIS 9 for the lower part (S4 and S3) and was coeval with MIS 7 for the upper part (S1), considering that in cold areas like the Swabian Jura, speleothems grow during interglacial periods. They confirm that the karstic system was functional starting at least from MIS 10-9. The U-series age obtained from the youngest part of the flowstone allows to indirectly constrain, by giving a *terminus post quem*, the beginning of cave occupation to ca 230 ka.

ESR ages can be compared with ^{14}C ages obtained from bones for GHs AU, D and E (**Tab. 1**). Except for the two problematic ages obtained from GHs D2 and E (12 ± 1 ka and 15 ± 3 ka, respectively), discarded from the interpretation due to the reasons mentioned above, ages obtained for the Middle Palaeolithic levels range from 46 ± 9 ka (GH K) to 33 ± 5 ka (GH D). Ages are reproducible for both GHs D and K. They range from 46 ± 9 ka to 38 ± 7 ka for GH K, and from 37 ± 6 ka to 33 ± 5 ka for GH D. Weighted mean ages (calculated with a weight of $1/\sigma^2$) are 40 ± 5 ka (GH K) and 35 ± 3 ka (GH D). They are however slightly younger than the ^{14}C date (1σ) obtained from GH D (44.1 ± 0.5 ka cal BP) (**Fig. 6**). The age obtained for the Early Aurignacian level (GH Au, 34 ± 11 ka), is in agreement with previous ^{14}C ages. The ESR ages, together with ^{14}C ages, point to cave occupation by Neanderthals during MIS 3. According ^{14}C ages, the end of Neanderthal presence could be thus related to Heinrich Stadial 4, around 40-38 ka.

6. Conclusions

ESR dating of fossil tooth enamel and U-series dating of a flowstone were conducted in order to establish the chronostratigraphic framework of the Middle Palaeolithic levels of Hohlenstein-Stadel. The ESR ages, ranging from 46 ± 9 ka (GH K) to 33 ± 5 ka (GH D) for the Middle Palaeolithic levels, are in agreement with ^{14}C ages except for those obtained on GH D, and confirm, as an independent method, the chronology of these levels. In spite of the large error range, the results demonstrate the possibility to apply ESR dating to relatively young samples (i.e., Late Pleistocene) in heterogeneous dosimetric environments with gravels, large limestone blocks and clays. Due to the low U-content in the dental tissues, the precision of the ages relies exclusively on the precision of the environmental dose rate. The results confirm the importance to apply a multi-method approach, the best way leading towards a precise chronology for the Middle Palaeolithic occupation. The U-series ages obtained on the flowstone indirectly date the beginning of occupation at the cave. The age

obtained from the upper part of the flowstone (229 ± 10 ka), directly overlying a sterile level located at the base of the sequence (GH M), must be considered as a *terminus post quem*. It seems that the karst was active starting from MIS 10-9 (around 350 ka). The ESR ages reported in this study, together with ^{14}C ages obtained previously, suggest that Neanderthals occupied the cave during MIS 3. Thus, these populations would have been among the last ones who settled in the Swabian Jura before being replaced by early *Homo sapiens*, as suggested by the presence of Aurignacian layers in several sites of the region.

Acknowledgments

This work was part of a PhD thesis funded by the French Ministery of Higher Education and Research, carried out at the MNHN. We thank E. Douville (LSCE) for providing access to ICP-QMS in LSCE and L. Bordier (LSCE) for performing the measurements.

Figures

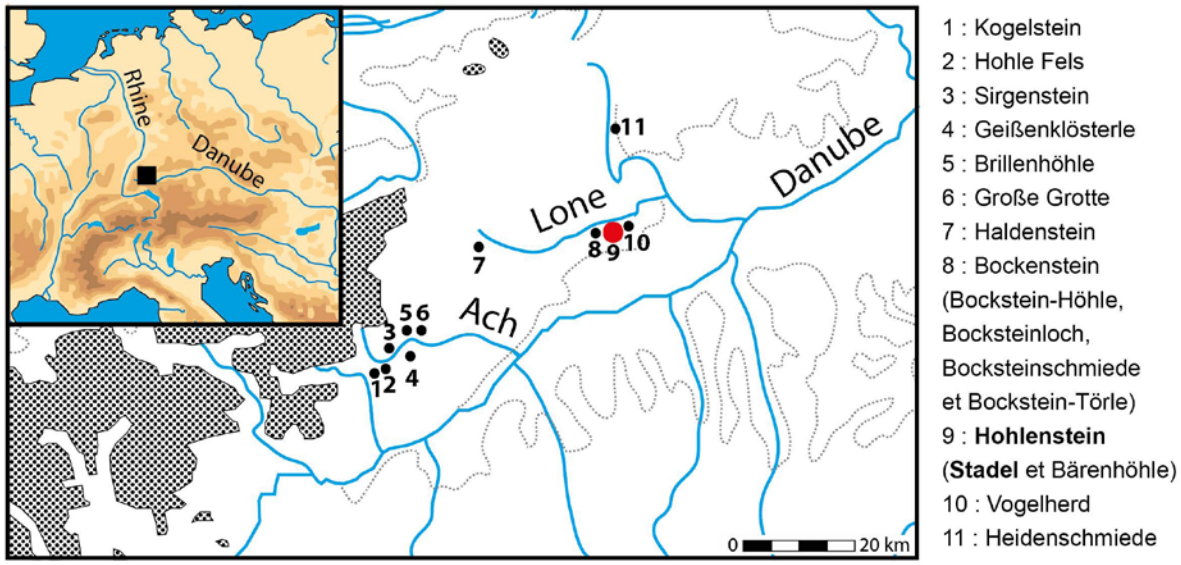

Fig. 1. Location of Hohlenstein-Stadel (red dot) and other Upper Pleistocene sites (black dot) in the Ach and Lone Valleys, Swabian Jura (Baden-Württemberg, Germany). Modified from Conard (2011).

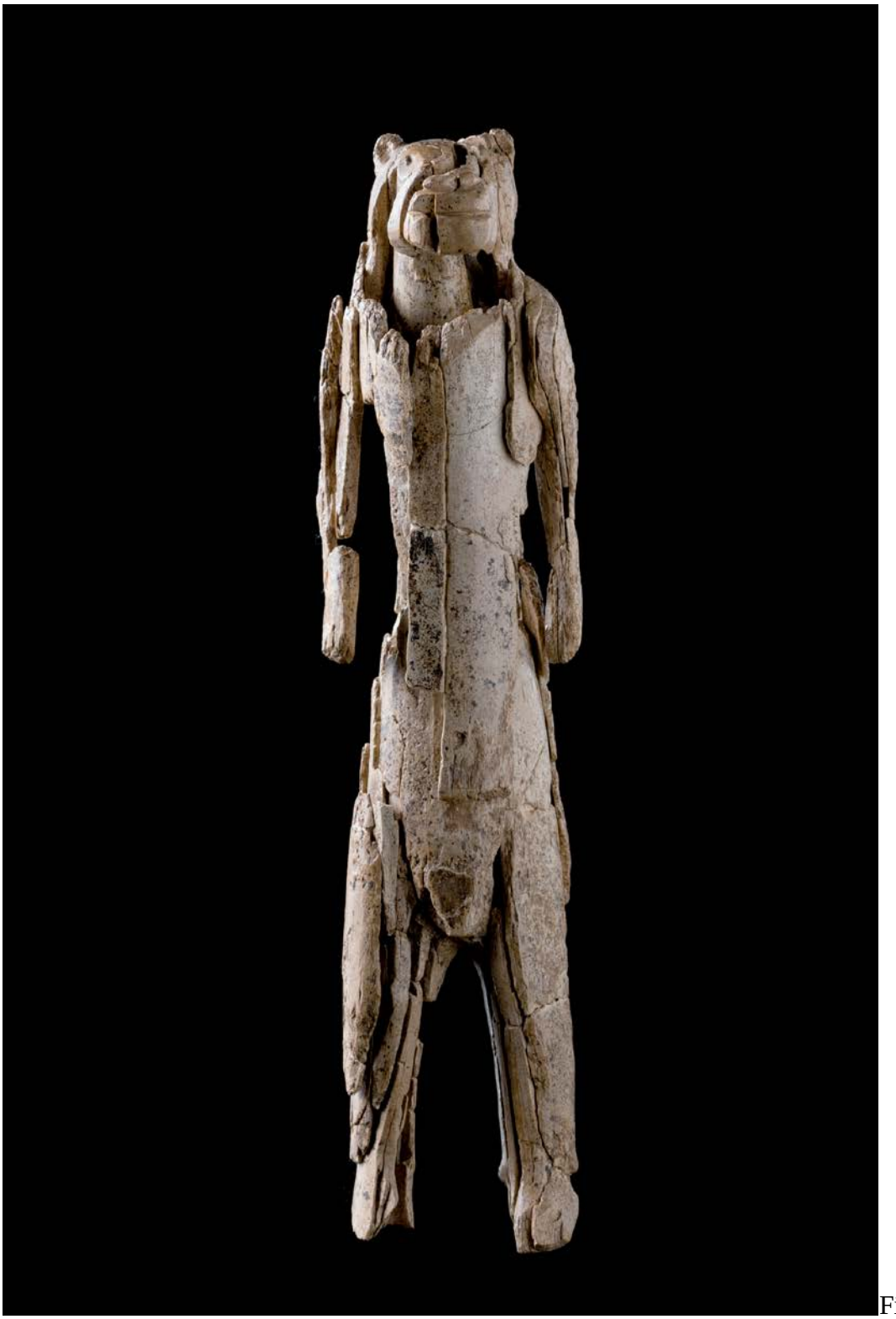

Fig. 2. Statuette of the Lion Man after the 2013 restoration. © Museum Ulm and State Office for Cultural Heritage Baden-Wuerttemberg. Photo by Y. Mühleis.

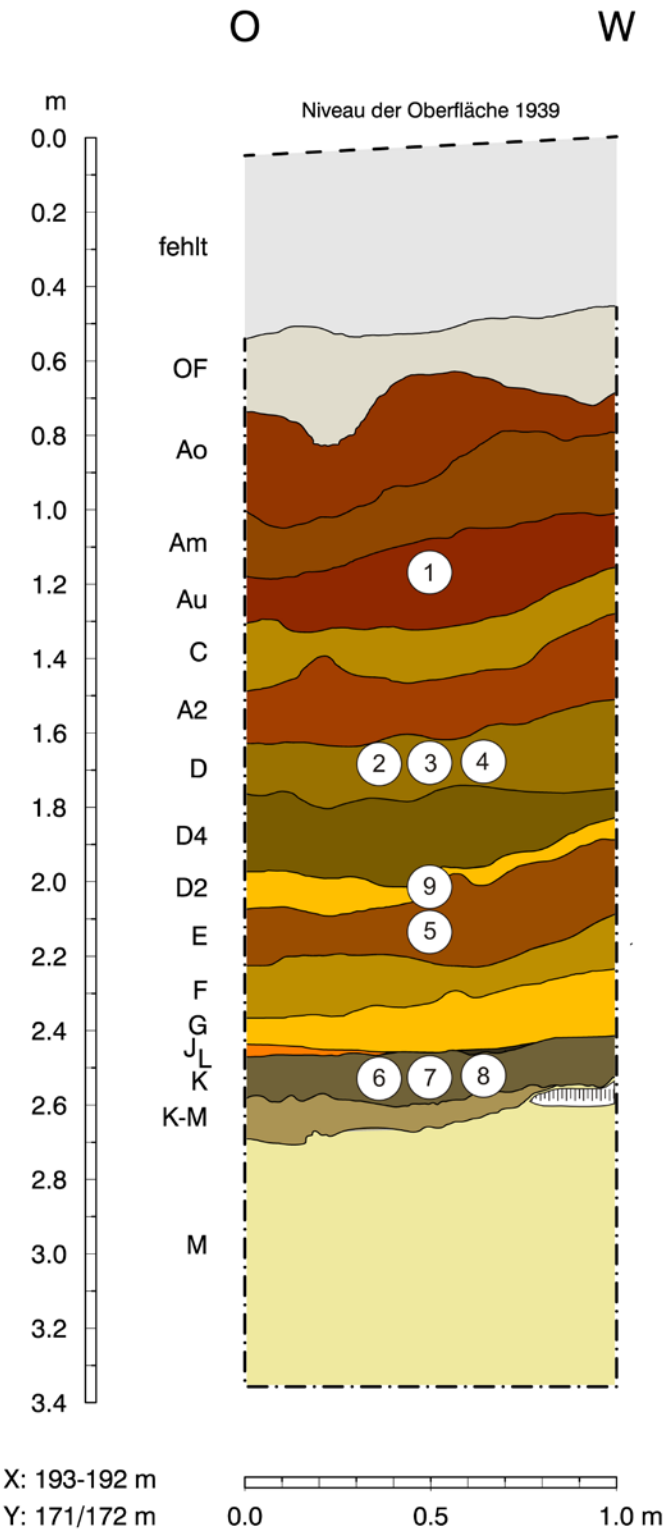

Fig. 3. Stratigraphic sequence of the new excavations from 2009-2013 and location of the teeth samples (east-west view). Numbers correspond to teeth sample; the speleothem is represented by the crosshatched formation, underlying GH K/M. © State Office for Cultural Heritage Baden-Württemberg.

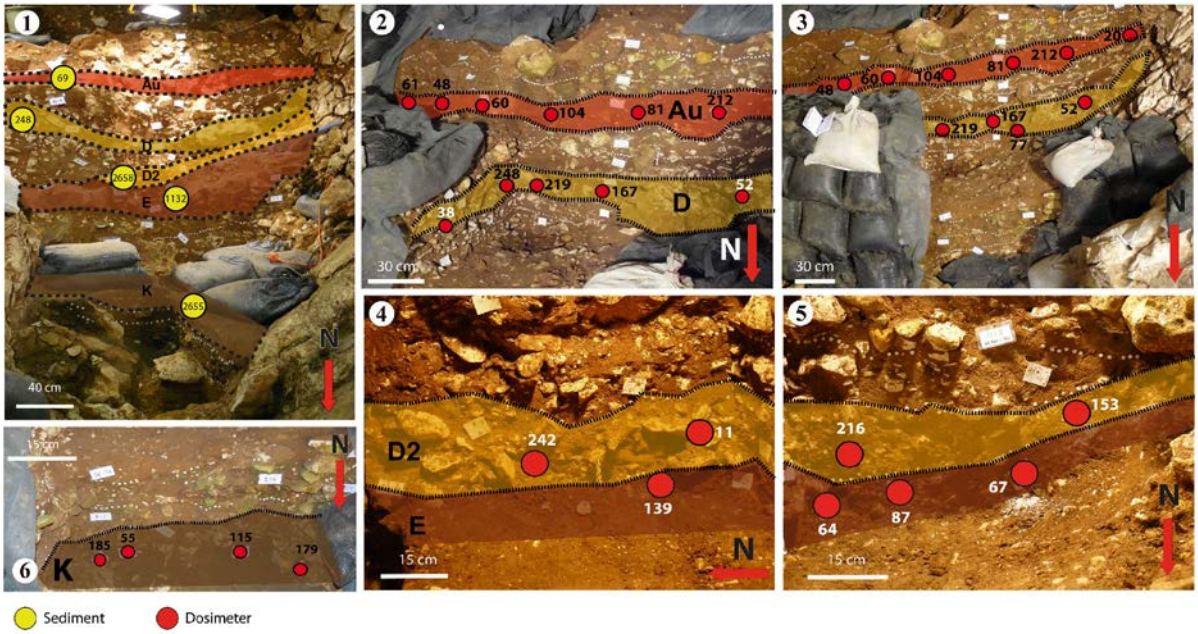

Fig. 4. Location of the dosimeters and sediment samples in the south and east sections. 1. General view of the stratigraphic sequence; 2 and 3. Zoom on GHs Au and D; 4 and 5. Zoom on GHs D2 and E*; 6. Zoom on GH K*. *Limit of the excavation area.

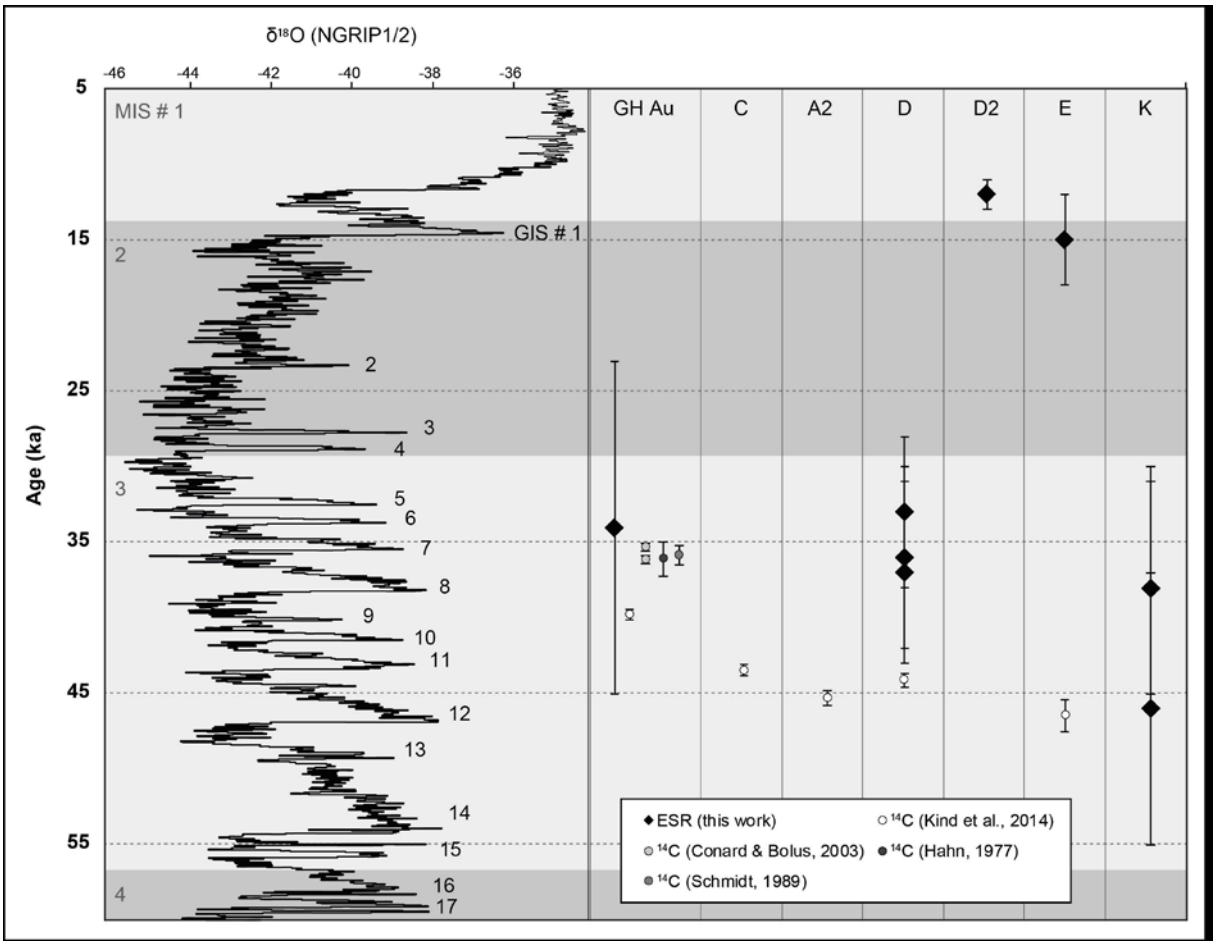

Fig. 5. a) Graphic representation of the ESR and ^{14}C ages obtained for Hohlenstein-Stadel as a function of the $\delta^{18}O$ variations (NGRIP data from Rasmussen et al., 2014) and available on http://www.iceandclimate.nbi.ku.dk/data). ^{14}C ages are calibrated using IntCal13 (Reimer et al., 2013) and Oxcal 4.3 (Bronk Ramsey, 2009).

Tables

GH	AH	Techno-complex	Sedimentology	Lab N°	^{14}C age (years)	δ^{13}C	Age cal BP (years)[1]
OF	OF	-	surface level (backdirt)				
Ao	1o	Aurignacian	clayey silt	ETH-41231	31,950 ± 210	-18.5 ± 1.1	36109-35627
Am	1m	Aurignacian	clayey silt	ETH-41232	33,390 ± 245	-21.1 ± 1.1	38244-37316
Au	1u	Aurignacian	clayey silt	ETH-38797	35,185 ± 270	-23.0 ± 1.1	40100-39418
C	3	Middle Palaeolithic	silty clay	ETH-38798	39,805 ± 420	-22.4 ± 1.1	43852-43072
A2	4	Middle Palaeolithic	Varved deposit with alternance of clay, silt and clay	ETH-38799	41,920 ± 545	-23.2 ± 1.1	45765-44814
D	5	Middle Palaeolithic	silty clay	ETH-38800	40,560 ± 480	-22.3 ± 1.1	44580-43643
D4	5b	Middle Palaeolithic	clayey silt				
D2	5a	Middle Palaeolithic	clayey silt				
E	6	Middle Palaeolithic	clayey silt	ETH-41234	46,440 ± 1050	-21.4 ± 1.1	Out of range
F	7	Middle Palaeolithic	clayey silt				
G	8	Middle Palaeolithic	clayey silt				
J	10	Middle Palaeolithic	silt				
K	11	Middle Palaeolithic	silt				
L	12	Middle Palaeolithic	silt				
K/M	13	Middle Palaeolithic	silt				
M	13	Sterile	sand and silt				

Tab 1. Geological (GH) and archaeological (AH) horizons, cultural attribution, sedimentology and radiocarbon ages (Kind et al., 2014) obtained on Hohlenstein-Stadel stratigraphic sequence.

[1]The calibration of radiocarbon ages on bones samples (with 1 σ uncertainty) was made using Oxcal v.4.3 (Bronk Ramsey, 2009) using IntCal 13 (Reimer et al., 2013).

Sample	Lab. N°	GH	AH	Square	X (m)	Y (m)	Z (m)	Taxon	Grain size (µm)[1]
Tooth	HS 01	Au	1u	192/172	191,8	171,52	475,08	*Equus*	0-200
Sediment	HS.sed.69	Au	1u	194/171	193,5	170,94	474,96	-	
Tooth	HS 02	D	5	193/172	192,5	171,44	474,52	*Equus*	100-200
Tooth	HS 03	D	5	193/173	192,7	171,93	474,52	*Equus*	0-200
Tooth	HS 04	D	5	193/172	192,9	171,69	474,56	*Equus*	100-200
Sediment	HS.sed.248	D	5	195/172	194,2	171,4	474,63	-	
Tooth	HS 09	D2	5a	193/172	192,8	171,61	474,11	*Rhinoceros*	100-200
Sediment	HS.sed.2658	D2	5a	193/173	193	172,02	474,19	-	
Tooth	HS 05	E	6	193/173	192,2	172,46	474,27	*Equus*	100-200
Sediment	HS.sed.1132	E	6	193/172	192,2	171,57	474,13	-	
Tooth	HS 06	K	11	193/173	192,3	172,16	473,74	*Equus*	0-200
Tooth	HS 07	K	11	193/173	192,3	172,24	473,74	*Equus*	100-200
Tooth	HS 08	K	11	193/173	192,2	172,43	473,68	*Equus*	100-100
Sediment	HS.sed.2655	K	11	193/173	192,5	172,11	473,62	-	-
Flowstone	HS.S1	M	13	194/174	193,5	173,22	473,73	-	-
Flowstone	HS.S3	M	13	194/174	193,5	173,33	473,65	-	-
Flowstone	HS.S4	M	13	194/174	193,5	173,3	473,64	-	-

Tab. 2. Samples number, stratigraphic attribution, coordinates (above the sea level) and taxonomic determination. [1]This column refers to the grain size used for ESR analyses.

Lab. N°	GH	D_e (Gy)	Dose rate (µGy/a)			Age (ka)
			Sediment (β + γ) + cosmic	Tooth (α + β)	Total	
HS 01	Au	14.12 ± 0.67	410 ± 134	5 ± 2	415 ± 134	**34 ± 11**
HS 02	D	11.99 ± 0.21	319 ± 53	3 ± 1	322 ± 53	**37 ± 6**
HS 03	D	11.84 ± 0.53	319 ± 53	6 ± 1	325 ± 53	**36 ± 6**
HS 04	D	10.47 ± 0.28	319 ± 53	-	319 ± 53	**33 ± 5**
HS 09	D2	12.98 ± 0.47	1035 ± 98	-	1035 ± 98	**12 ± 1**
HS 05	E	14.50 ± 0.42	941 ± 207	3 ± 1	944 ± 207	**15 ± 3**
HS 06	K	35.67 ± 1.70	774 ± 155	4 ± 1	778 ± 194	**46 ± 9**
HS 07	K	29.55 ± 1.05	774 ± 155	6 ± 2	780 ± 194	**38 ± 8**
HS 08	K	32.39 ± 0.92	848 ± 155	1 ± 1	849 ± 194	**38 ± 7**

Tab. 3. Equivalent doses (D_e), dose rates and ESR ages (1 σ) obtained for the teeth samples.

Lab. N°	GH	Tissu	^{238}U (ppm)	$^{234}U/^{238}U$	$^{230}Th/^{234}U$	$^{230}Th/^{232}Th$	Enamel (Ini. thick, µm)	Side 1 (Rem. thick., µm)	Side 2 (Rem. thick., µm)
HS 01	Au	E	0.0118 ± 0.0001	1.216 ± 0.007	0.391 ± 0.352	12.83 ± 11.47	839 ± 84	80 ± 8	58 ± 6
		D	0.1792 ± 0.0003	1.245 ± 0.031	0.249 ± 0.033	5.83 ± 0.76			
		C	0.1239 ± 0.0004	1.489 ± 0.061	nd	nd			
HS 02	D	E	0.0030 ± 0.0001	1.516 ± 0.498	nd	nd	1144 ± 114	79 ± 8	57 ± 6
		D	0.0723 ± 0.0007	1.166 ± 0.043	0.320 ± 0.060	5.30 ± 0.99			
		C	0.2018 ± 0.0085	1.314 ± 0.152	nd	17.24 ± 4.46			
HS 03	D	E	0.0125 ± 0.0001	1.280 ± 0.083	0.580 ± 0.142	46.51 ± 11.40	1353 ± 135	169 ± 17	164 ± 16
		D	0.0875 ± 0.0023	2.048 ± 0.842	0.196 ± 0.084	7.64 ± 0.86			
		C	0.4222 ± 0.0090	1.209 ± 0.087	0.299 ± 0.018	13.43 ± 0.78			
HS 04	D	E	0.0025 ± 0.0001	1.267 ± 0.093	nd	nd	1198 ± 120	129 ± 13	98 ± 10
		D	0.0300 ± 0.0003	1.196 ± 0.072	1.201 ± 0.092	13.49 ± 0.64			
		C	0.0604 ± 0.0007	1.209 ± 0.069	0.333 ± 0.028	3.94 ± 0.25			
HS 05	D2	E	0.0053 ± 0.0001	1.531 ± 0.344	nd	nd	1094± 109	60 ± 6	58 ± 6
		D	0.0380 ± 0.0001	1.228 ± 0.035	0.475 ± 0.073	26.46 ± 3.55			
		C	0.2717 ± 0.0038	1.306 ± 0.072	0.366 ± 0.019	7.77 ± 0.39			
HS 06	C	E	0.0029 ± 0.0001	1.294 ± 0.137	nd	nd	1393 ± 139	89 ± 9	85 ± 8
		D	0.0152 ± 0.0001	1.270 ± 0.063	0.467 ± 0.096	8.78 ± 1.80			
		C	0.4324 ± 0.0266	1.435 ± 0.348	0.332 ± 0.025	16.39 ± 0.59			
HS 07	K	E	0.0026 ± 0.0001	1.733 ± 0.436	nd	nd	1384 ± 138	109 ± 11	48 ± 5
		D	0.0237 ± 0.0002	1.317 ± 0.042	0.332 ± 0.093	2.62 ± 0.73			
		C	0.5354 ± 0.0025	1.272 ± 0.037	0.131 ± 0.009	7.99 ± 0.49			
HS 08	K	E	0.0050 ± 0.0001	1.405 ± 0.200	nd	nd	1519 ± 152	136 ± 14	127 ± 13
		D	0.0386 ± 0.0002	1.317 ± 0.062	nd	nd			
HS 09	K	E	0.0032 ± 0.0001	1.478 ± 0.315	nd	nd	1678 ± 168	49 ± 5	41 ± 4
		D	0.0400 ± 0.0002	1.205 ± 0.020	0.734 ± 0.042	45.85 ± 2.63			

Tab. 4. U-Th data (U-content and isotopic ratios) obtained on the dental tissues and initial and removed thickness on side 1 (dentine) and side 2 (cement or sediment). nd = non determinable. E = enamel; D = dentine; C = cement.

Lab. N°	GH	^{238}U (ppm)	^{232}Th (ppm)	^{40}K (%)
HS.sed.69	Au	1.698 ± 0.090	6.091 ± 0.144	0.650 ± 0.013
HS.sed.248	D	1.566 ± 0.088	5.370 ± 0.140	0.619 ± 0.012
HS.sed.2658	D2	1.133 ± 0.094	6.156 ± 0.156	0.636 ± 0.014
HS.sed.1132	E	1.784 ± 0.134	9.317 ± 0.25	0.680 ± 0.019
HS.sed.2655	K	2.461 ± 0.134	9.288 ± 0.226	0.923 ± 0.019

Tab. 5. ^{238}U, ^{232}Th and ^{40}K content measured using laboratory gamma-ray spectrometry. Sediment numbers match with the ones presented in Fig. SI3.

GH	N°	Square	x	y	z	γ dose rate (µGy/a)	Mean value (µGy/a)[1]	Mean value (µGy/a)[2]
Au	60	194/172	193,25	171,00	475	223	452 ± 272	410 ± 134
Au	20	192/171	191,19	170,98	474,3	583		
Au	212	192/171	191,77	170,99	474,1	970*		
Au	61	195/171	194,02	170,90	474,9	461		
Au	104	193/171	192,76	170,96	475	145*		
Au	48	194/171	193,58	170,94	474,9	348		
Au	81	193/171	192,2	170,97	474,1	437		
D	52	192/172	191,6	171,05	474,6	401	351 ± 92	319 ± 53
D	219	193/172	192,82	171,00	474,5	330		
D	248	193/172	192,97	171,12	474,5	306		
D	38	193/172	192,98	171,75	474,5	256		
D	77	193/171	192,18	170,98	474,5	512*		
D	167	193/171	192,4	170,98	474,5	301		
D2	11	193/172	192,99	171,18	474,2	1128	1133 ± 213	1035 ± 98
D2	153	193/172	192,28	171,01	474,3	1430*		
D2	242	193/172	192,99	171,65	474,1	933		
D2	216	193/172	192,84	171,03	474,1	1043		
E	67	193/172	192,41	171,02	474,1	1087	873 ± 545	941 ± 207
E	87	193/172	192,71	171,03	474	162*		
E	64	193/172	192,91	171,08	474	1450*		
E	139	193/172	192,96	171,31	474	794		
K	55	193/173	192,75	172,04	473,7	774	983 ± 485	1179 ± 351
K	185	193/174	192,89	172,10	473,7	396*		
K	179	193/175	192,05	172,09	473,7	1368		
K	115	193/176	192,26	172,00	473,7	1395		

Tab. 6. In-situ gamma dosimetry: GH, dosimeter numbers (matching with the ones presented in Fig. 4), coordinates and dose rates (1mean value and standard deviation by GH; 2mean value and standard deviation excluding the extreme values by GH used for age calculation). *extreme values that do not fall within the range of the standard deviation.

Lab. N°	^{238}U (ppb)	^{234}U/^{238}U mes.	^{230}Th/^{234}U	^{230}Th/^{232}Th	Age (ka)	Corr. age (ka)*	^{234}U/^{238}U ini.
HS.S1	57.92 ± 0.03	1.152 ± 0.005	0.915 ± 0.006	20.54 ± 0.11	**235 ± 8**	**229 ± 10**	1.290 ± 0.015
HS.S3	160.14 ± 0.04	1.088 ± 0.001	0.957 ± 0.002	19.74 ± 0.04	**296 ± 4**	**290 ± 7**	1.199 ± 0.005
HS.S4	114.67 ± 0.05	1.118 ± 0.002	0.997 ± 0.002	29.78 ± 0.06	**356 ± 9**	**351 ± 10**	1.319 ± 0.013

Tab. 7. U-series data: ^{238}U content, activity ratios (measured and initial ^{234}U/^{238}U, ^{230}Th/^{232}Th and ^{230}Th/^{234}U) and uncorrected and corrected ages (2 σ) obtained on the flowstone samples. Ages were corrected for detrital thorium following Kaufman and Broecker (1965) and using a ^{230}Th/^{232}Th initial ratio of the detrital phase of 1.5 ± 50%

References

Adamiec, G., Aitken, M.J., 1998. Dose-rate conversion factors: update. Ancient TL 16, 37-50.

Beutelspacher, T., Ebinger-Rist, N., Kind, J.-C., 2010. Neue Funde aus der Stadelhöhle im Hohlenstein bei Asselfingen. Archäologische Ausgrabungen in Baden-Württemberg, 65-70.

Beutelspacher, T., Kind, J.-C., 2011. Auf der Suche nach Fragmenten des Löwenmenschen in der Stadelhöhle im Hohlenstein bei Asselfingen. Archäologische Ausgrabungen in Baden-Württemberg, 66-70.

Bischoff, J.L., Rosenbauer, R.J., 1981. Uranium Series Dating of Human Skeletal Remains from the Del Mar and Sunnyvale Sites, California. Science 213, 1003-1005.

Brennan, B.J., Rink, W.J., McGuirl, E.L., Schwarcz, H.P., Prestwich, W.V., 1997. Beta doses in tooth enamel by "one-group" theory and the ROSY ESR dating software. Radiation Measurements 27, 307-314.

Bronk Ramsey, C., 2009. Bayesian Analysis of Radiocarbon Dates. Radiocarbon 51, 337-360.

Conard, N.J., 2003. Palaeolithic ivory sculptures from southwestern Germany and the origins of figurative art. Nature 426, 830-832.

Conard, N.J., 2009. A female figurine from the basal Aurignacian of Hohle Fels Cave in southwestern Germany. Nature 459, 248-252.

Conard, N.J., 2011. The Demise of the Neanderthal Cultural Niche and the Beginning of the Upper Paleolithic in Southwestern Germany, in: Conard, N.J., Richter, J. (Eds.), Neanderthal Lifeways, Subsistence and Technology. Springer Netherlands, pp. 223-240.

Conard, N.J., Bolus, M., 2003. Radiocarbon dating the appearance of modern humans and timing of cultural innovations in Europe: new results and new challenges. Journal of Human Evolution 44, 331-371.

Conard, N.J., Bolus, M., 2006. The Swabian Aurignacian and its Role in European Prehistory, in: Bar-Yosef, O., Zilhão, J. (Eds.), Towards a Definition of the Aurignacian. Instituto Português de Arqueologia, Lisbonne, pp. 211-239.

Conard, N.J., Bolus, M., 2008. Radiocarbon dating the late Middle Paleolithic and the Aurignacian of the Swabian Jura. Journal of Human Evolution 55, 886-897.

Conard, N.J., Malina, M., Munzel, S.C., 2009. New flutes document the earliest musical tradition in southwestern Germany. Nature 460, 737-740.

d'Errico, F., 2003. The invisible frontier. A multiple species model for the origin of behavioral modernity. Evolutionary Anthropology: Issues, News, and Reviews 12, 188-202.

Douville, E., Sallé, E., Frank, N., Eisele, M., Pons-Branchu, E., Ayrault, S., 2010. Rapid and accurate U–Th dating of ancient carbonates using inductively coupled plasma-quadrupole mass spectrometry. Chemical Geology 272, 1-11.

Floss, H., 2017. Same as it ever was? The Aurignacian of the Swabian Jura and the origins of Palaeolithic art. Quaternary International.

Grün, R., 2009. The DATA program for the calculation of ESR age estimates on tooth enamel. Quaternary Geochronology 4, 231-232.

Grün, R., Joannes-Boyau, R., Stringer, C., 2008. Two types of CO_2^- radicals threaten the fundamentals of ESR dating of tooth enamel. Quaternary Geochronology 3, 150-172.

Grün, R., Katzenberger-Apel, O., 1994. An alpha irradiator for ESR dating. Ancient TL 12, 35-38.

Grün, R., Schwarcz, H.P., Chadam, J., 1988. ESR dating of tooth enamel: Coupled correction for U-uptake and U-series disequilibrium. International Journal of Radiation Applications and Instrumentation. Part D. Nuclear Tracks and Radiation Measurements 14, 237-241.

Hahn, J., 1971. La statuette masculine de la Grotte du Hohlenstein-Stadel (Wurtemberg). L'Anthropologie 75, 233-244.

Hahn, J., 1977. Aurignacien, das ältere Jungpaläolithikum im Mittel- und Osteuropa. Böhlau, Köln-Wien.

Higham, T., Basell, L., Jacobi, R., Wood, R., Ramsey, C.B., Conard, N.J., 2012. Testing models for the beginnings of the Aurignacian and the advent of figurative art and music:

the radiocarbon chronology of Geißenklösterle. Journal of Human Evolution 62, 664-676.

Kaufman, A., Broecker, W., 1965. Comparison of Th^{230} and C^{14} ages for carbonate materials from Lakes Lahontan and Bonneville. Journal of geophysical Research, 70, 4039-4054.

Kind, J.-C., Ebinger-Rist, N., Wolf, S.F., Beutelspacher, T., Wehrberger, K., 2014. The Smile of the Lion Man. Recent Excavations in Stadel Cave (Baden-Württemberg, south-western Germany) and the Restoration of the Famous Upper Palaeolithic Figurine. Quartär 61, 129-145.

Kitagawa, K., Krönneck, P., Conard, N.J., Münzel, S.C., 2012. Exploring Cave Use and Exploitation Among Cave Bears, Carnivores and ominins in the Swabian Jura, Germany Journal of Taphonomy 10, 439-461.

Krönneck, P., Niven, L., Uerpmann, H.P., 2004. Middle Palaeolithic subsistence in the Lone Valley (Swabian Alb, southern Germany). International Journal of Osteoarchaeology 14, 212-224.

Mellars, P., 2005. The impossible coincidence. A single-species model for the origins of modern human behavior in Europe. Evolutionary Anthropology: Issues, News, and Reviews 14, 12-27.

Peresani, M., Cremaschi, M., Ferraro, F., Falguères, C., Bahain, J.-J., Gruppioni, G., Sibilia, E., Quarta, G., Calcagnile, L., Dolo, J.-M., 2008. Age of the final Middle Palaeolithic and Uluzzian levels at Fumane Cave, Northern Italy, using ^{14}C, ESR, $^{234}U/^{230}Th$ and thermoluminescence methods. Journal of Archaeological Science 35, 2986-2996.

Pons-Branchu E., Douville E., Roy-Barman M., Dumont E., Branchu E., Thil F., Frank N., Bordier L., Borst W., 2014. A geochemical perspective on Parisian urban history based on U-Th dating, laminae counting and yttrium and REE concentrations of recent carbonates in underground aqueducts. Quaternary Geochronology 24, 44-53.

Prescott, J.R., Hutton, J.T., 1994. Cosmic ray contributions to dose rates for luminescence and ESR dating: Large depths and long-term time variations. Radiation Measurements 23, 497-500.

Rasmussen, S.O., Bigler, M., Blockley, S.P., Blunier, T., Buchardt, S.L., Clausen, H.B., Cvijanovic, I., Dahl-Jensen, D., Johnsen, S.J., Fischer, H., Gkinis, V., Guillevic, M., Hoek, W.Z., Lowe, J.J., Pedro, J.B., Popp, T., Seierstad, I.K., Steffensen, J.P., Svensson, A.M., Vallelonga, P., Vinther, B.M., Walker, M.J.C., Wheatley, J.J., Winstrup, M., 2014. A stratigraphic framework for abrupt climatic changes during the Last Glacial period based on three synchronized Greenland ice-core records: refining

and extending the INTIMATE event stratigraphy. Quaternary Science Reviews 106, 14-28.

Reimer, P.J., Bard, E., Bayliss, A., Beck, J.W., Blackwell, P.G., Bronk Ramsey, C., Buck, C.E., Cheng, H., Edwards, R.L., Friedrich, M., Grootes, P.M., Guilderson, T.P., Haflidason, H., Hajdas, I., Hatté, C., Heaton, T.J., Hoffmann, D.L., Hogg, A.G., Hughen, K.A., Kaiser, K.F., Kromer, B., Manning, S.W., Niu, M., Reimer, R.W., Richards, D.A., Scott, E.M., Southon, J.R., Staff, R.A., Turney, C.S.M., van der Plicht, J., 2013. IntCal13 and Marine13 Radiocarbon Age Calibration Curves 0–50,000 Years cal BP. Radiocarbon 55, 1869-1887.

Richard, M., Falguères, C., Pons-Branchu, E., Bahain, J.J., Voinchet, P., Lebon, M., Valladas, H., Dolo, J.M., Puaud, S., Rué, M., Daujeard, C., Moncel, M.H., Raynal, J.P., 2015. Contribution of ESR/U-series dating to the chronology of late Middle Palaeolithic sites in the middle Rhône valley, southeastern France. Quaternary Geochronology 30, 529-534.

Richter, D., Dombrowski, H., Neumaier, S., Guibert, P., Zink, A.C., 2010. Environmental gamma dosimetry with OSL of α-Al_2O_3:C for in situ sediment measurements. Radiatiation Protection Dosimetry 141, 27-35.

Schmid, E., 1989. Die altsteinzeitliche Elfenbeinstatuette aus der Höhle Stadel im Hohlenstein bei Asselfingen, Alb-Donau-Kreis. With contributions by Hahn, J., Wolf, U. Fundber. Baden-Württemberg 14, 33-108.

Yokoyama, Y., Falguères, C., Quaegebeur, J.P., 1985. ESR dating of quartz from quaternary sediments: First attempt. Nuclear Tracks and Radiation Measurements (1982) 10, 921-928.